Large scale 3D inversion of HEM data using a moving footprint

*Leif H. Cox * and Michael S. Zhdanov, University of Utah*

SUMMARY

Helicopter electromagnetic surveying is a standard reconnaissance method in the mining industry. Typical surveys may cover tens to hundreds of square kilometers with hundreds of thousands of multi-frequency soundings. Interpreting this volume of data is problematic. Yet each sounding location is sensitive to an area of less than 1 km^2, not the entire survey area. We suggest an inversion scheme, based on the integral equation method, in which the entire survey is inverted simultaneously with each transmitter-receiver pair being sensitive only to a relatively small area around each sounding location. We show that this method is as accurate as standard integral equation inversion methods, yet it inverts the data much faster. The technique is able to invert entire HEM surveys with over 500,000 inversion cells and tens of thousands of transmitter positions in less than one day on a single PC.

INTRODUCTION

Helicopter electromagnetic (HEM) exploration is a very powerful tool for surveying large areas rapidly and relatively inexpensively. Surveys may cover hundreds of line-kilometers with multi-component and multi-frequency soundings every few meters. This enables collecting huge amounts of data about the electrical properties of the earth. However, interpreting the massive amounts of data gathered poses a significant challenge. Any 3D inversion must contain hundreds of thousands of cells to cover the entire domain. Computationally, the problem is exacerbated by the fact that, for each sounding point, a new electric field is introduced into the earth. This requires solving an enormous number of equations simultaneously for a full rigorous 3D inversion.

It is widely known that airborne data include a relatively limited footprint area (Reid et al., 2006; Beamish, 2003; Liu and Becker, 1990). These papers have been devoted to exploring these footprint sizes for survey design, resolution, and applicability of 1D inversion algorithms. We use a similar idea in the context of 3D inversion.

We extend two existing HEM inversion methods to include a moving footprint, i.e., allowing sensitivity of model cells only within the airborne footprint of a transmitter-receiver pair. This effectively creates sparse inverse and forward operators to enable practical inversion of full frequency-domain surveys. The algorithms this technique is applied to are the localized quasi-linear inversion (LQL) (Zhdanov and Tartaras, 2002) and a rigorous integral equation method (Cox and Zhdanov, 2006).

METHODS

Integral equation

In the integral equation formulation, we separate the fields into a normal part, associated with a layered earth background, and an anomalous part, which corresponds to some anomalous conductivity distribution ($\Delta\sigma$) inside an anomalous domain:

$$\mathbf{H} = \mathbf{H}^a + \mathbf{H}^b, \tag{1}$$

$$\mathbf{E} = \mathbf{E}^a + \mathbf{E}^b. \tag{2}$$

For a known survey configuration and a known layered earth conductivity, one can compute the normal fields analytically. In HEM, equation (1) corresponds to a field equation, or the response of the receivers. Equation (2) is the electric field inside the anomalous domain. The integral equations for the anomalous fields are a function of the total field, the layered earth conductivity, and the anomalous conductivity, and are given by:

$$\mathbf{H}^a = \iiint_D \hat{\mathbf{G}}_{\mathbf{H}}[\Delta\sigma\mathbf{E}]dV \approx \mathbf{G}_H[\Delta\sigma\mathbf{E}], \tag{3}$$

$$\mathbf{E}^a = \iiint_D \hat{\mathbf{G}}_{\mathbf{E}}[\Delta\sigma\mathbf{E}]dV \approx \mathbf{G}_E[\Delta\sigma\mathbf{E}]. \tag{4}$$

where $\hat{\mathbf{G}}_{(\mathbf{H}|\mathbf{E})}$ are the Green's functions for the magnetic or electric fields and $\mathbf{G}_{(\mathbf{H}|\mathbf{E})}$ are the corresponding Green's tensors.

While it is well known how to solve this nonlinear equation, a rigorous solution for the anomalous electric field is very time-consuming to find. In the inverse problem, which we will solve here, this is the computational bottleneck. Several approximations have been proposed to speed this solution, including quasi-analytic (QA) (Zhdanov and Hursan, 2000), localized non-linear (LN) (Habashy et al., 1993), and quasi-linear (QL) (Zhdanov and Fang, 1996). In this paper, we follow the localized quasi-linear (LQL) approximation (Zhdanov and Tartaras, 2002) for our approximate solution, and a full rigorous method (Cox and Zhdanov, 2006)

Localized quasi-linear background

The LQL assumption states that the anomalous electric field at any given location in the anomalous domain is linearly proportional to the background field at that location through a reflectivity tensor, λ. This reflectivity tensor is independent of the source location, so each location has a unique reflectivity tensor even though the survey may contains thousands of transmitter positions. The LQL approximation is given by:

$$\mathbf{E}_I^a \approx \hat{\lambda}\mathbf{E}_\mathbf{I}^\mathbf{b}, \tag{5}$$

where I is the transmitter index. This greatly simplifies and speeds computation of the anomalous fields. The inversion formulation based on this assumption is given as follows.

Using equation (5), we can see that the total electric field is given by:

$$\mathbf{E}_I = \mathbf{E}_I^b + \widehat{\lambda}\mathbf{E}_I^b = (\widehat{\mathbf{I}} + \widehat{\lambda})\mathbf{E}_I^b. \tag{6}$$

Following Zhdanov and Tartaras (2002), we introduce a new tensor function:

$$\widehat{\mathbf{m}}(\mathbf{r}) = \Delta\sigma_{LQL}(\mathbf{r})\left(\widehat{\mathbf{I}} + \widehat{\lambda}(\mathbf{r})\right), \tag{7}$$

which we call a modified material property tensor.

Substituting equation (6) into equation (3), and using (7), we can write:

$$\mathbf{H}_I^a(\mathbf{r}_j) = \mathbf{G}_H\left[\widehat{\mathbf{m}}(\mathbf{r}) \cdot \mathbf{E}_I^b(\mathbf{r})\right]. \tag{8}$$

We can solve the linear equation (8) with respect to $\widehat{\mathbf{m}}(\mathbf{r})$, which is source independent.

The reflectivity tensor, $\widehat{\lambda}(\mathbf{r})$, is determined based on condition (9),which constitutes an important step of the LQL inversion:

$$\left\|\widehat{\lambda}(\mathbf{r}) - \mathbf{G}_E\left[\widehat{\mathbf{m}}(\mathbf{r})\right]\right\|_{L_2(D)} = \min. \tag{9}$$

Knowing $\widehat{\lambda}(\mathbf{r})$ and $\widehat{\mathbf{m}}(\mathbf{r})$, we can find $\Delta\sigma(\mathbf{r})$ from equation (7) by using the least-squares method (Zhdanov and Tartaras, 2002).

We can rewrite equation (8) using matrix notations:

$$\mathbf{d} = \mathbf{G}\mathbf{m}. \tag{10}$$

Here $\mathbf{m}$ is the vector-column of the modified material property tensor $\widehat{\mathbf{m}}$, $\mathbf{d}$ is the vector-column of the field data, and $\mathbf{G}$ is the matrix of the linear operator defined by equation (8).

Rigorous inversion background

The rigorous inversion method (Cox and Zhdanov, 2006) begins with the results of the LQL method to obtain a starting conductivity distribution and electric field. The initial electric field is found from:

$$\mathbf{E}_I^{(0)} = \mathbf{G}_E\left[\widehat{\mathbf{m}}\cdot\mathbf{E}_I^b\right] + \mathbf{E}_I^b. \tag{11}$$

Equation (3) is then inverted for a new conductivity distribution.

$$\mathbf{H}_I^a = \mathbf{G}_H[\Delta\sigma^{(1)}\cdot\mathbf{E}_I^{(0)}] \tag{12}$$

This process of updating the electric field (equation [13]) and inverting for a new conductivity distribution (equation [14]) continues until the desired misfit is reached:

$$\mathbf{E}_I^{(n)} = \mathbf{G}_E\left[\Delta\sigma^{(n)}\cdot\mathbf{E}_I^{(n-1)}\right] + \mathbf{E}_I^b \tag{13}$$

$$\mathbf{H}_I^a = \mathbf{G}_H\left[\Delta\sigma^{(n+1)}\cdot\mathbf{E}_I^{(n)}\right]. \tag{14}$$

Equation (14) can be reduced to the notation of equation (10), where $\mathbf{H}_I^a$ is equivalent to $\mathbf{d}$, $\mathbf{G}$ is $\mathbf{G}_H\cdot\mathbf{E}_I^{(n)}$, and $\Delta\sigma^{(n+1)}$ are the model parameters.

We use the re-weighted regularized conjugate gradient method to solve the system of the linear equations (10), which is based on the Tikhonov regularization technique (Zhdanov, 2002).

Modified forward and inverse operator

Consider the inversion domain shown in Figure 1. In the original formulation, every sounding location would be sensitive to every cell in the inversion domain.

If one examines the original forward operator (equation [10]), it can be expressed in indicial notation as:

$$d_i = \sum_{j=1}^{Nc}\mathbf{G}_{ij}m_j. \tag{15}$$

where N_c is the total number of cells in the domain. This summation includes all the cells, (j), in the inversion domain for each transmitter position, (i). But most of these cells do not contribute to the measured response and we do not need to include them in the summation. Referring to Figure 1, we now include only the cells in the shaded region for each transmitter. To accomplish this, equation (15) is modified to be, for our example:

$$d_i = \sum\mathbf{G}_{ij}m_j \tag{16}$$

where:

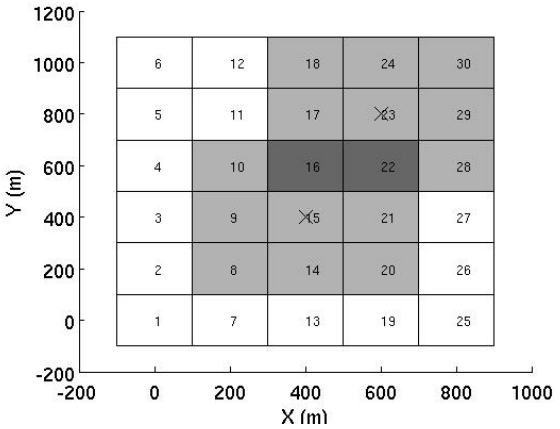

Figure 1: Example inversion domain. The cells are numbered for clarity and correspond to the text. The domain for the original inverse operator for each transmitter-receiver pairs is the entire domain shown. The windowed domain includes only the shaded regions for each of the two stations shown. There is a transmitter-receiver pair located above cell 15 and another above cell 23. These are called 1 and 2, respectively.

$$j = \begin{cases} 8,9,10,14,15,16,20,21,22 & \text{if } i=1; \\ 16,17,18,22,23,24,28,29,30 & \text{if } i=2 \end{cases}$$

with the numbers given for j corresponding to the cells shown in Figure 1.

Using the same logic, the inversion scheme may also be modified. In this manner, we do not take into account cells outside the footprint by simply excluding them from the summation. Thus, there is no need to calculate the Green's body-to-receiver tensors and background fields for these cells, and we avoid much of the computation in both forward modeling and inversion. Note that in this example domain, there would not be adequate coverage to find conductivity values for every cell. In a true survey, each cell would be within the footprint of multiple sounding locations.

In addition, one of the most time-consuming and memory-expensive parts of the inversion is the pre-computation of the body-to-body Green's tensors. Since the background model is horizontally layered, the body-to-body Green's tensors are horizontally invariant. Hence, these Green's tensors are identical for each sounding location, and only one set needs to be computed for a single transmitter position within a single footprint. These are then translated over the entire domain, vastly speeding up the computation and increasing the memory efficiency.

RESULTS

Synthetic example

Two conductive and two resistive bodies of varying size and depth have been placed in a homogenous half-space to test the moving footprint inversion algorithm. Flight lines were synthesized at an elevation of 30 meters with sounding locations every 50 m. The 16 flight lines were spaced 100 m apart. The synthetic model is shown in Figure 2. The survey is shown overlaid on the domain. Four frequencies were used: 900 and 7200 Hz Coplanar and 1000 and 5500 Hz Coaxial. Each channel contained 632 sounding locations, giving 2528 total stations. No noise was added to the data.

Large Scale 3D inversion

The inversion domain contained 70,000 total cells, each a cube 25 m on a side. In this example we used a 500 m x 500 m footprint for every transmitter position.

The rigorous inversion results using the moving footprint method are shown in Figure 3; note that it was not possible to invert the domain using the rigorous inversion without using a moving footprint. In this inversion the depth of the bodies are well constrained and the conductivities are close to the true values. Both a windowed and non-windowed LQL inversion were also performed on this synthetic model. The windowing did not affect the inversion results, but the windowed inversion was 10 times faster than than the standard method.

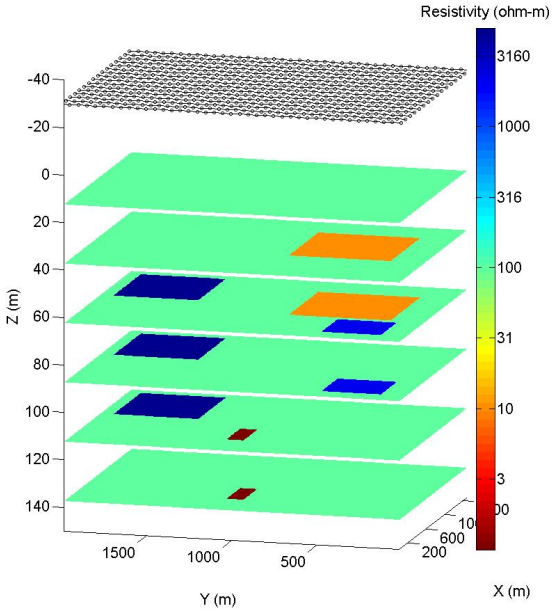

Figure 2: Locations of synthetic anomalies with flight lines overlaid.

We show that there is a large time and memory savings from "windowing" the inversion, even in this relatively small inversion area of 3 km^2.

Field Example

Survey and geologic background

The field data set is an AeroDat survey flown with five frequencies: 865, 4175, and 33000 Hz Coplanar and 935 and 4600 Hz Coaxial. This survey originally contained approximately 44,000 sounding locations per channel, for an approximate spacing of 3 m along line and 200 m line spacing. For this test, we have taken every 10^{th} data point. The survey was taken over a high sulfidation gold system in Mexico. Due to the highly silicified alteration areas surrounding the economic gold, the targets in this area are resistive.

Inversion results

We start with an isolated area to test the mechanics of the inversion algorithm. This area is shown in the box in Figure 4. The goal is to show that we can get accurate inversion results for this known geologic structure, then extend the inversion domain to the entire survey and show the inversion result in the isolated area does not change when using a moving footprint inversion. The inversion was run using approximately 100 sounding locations per channel, for a total of 500 soundings. The inversion domain was 2.8 km^2 with a depth range of 0 to 150 m. The inversion cells were 25 m cubes creating a total of

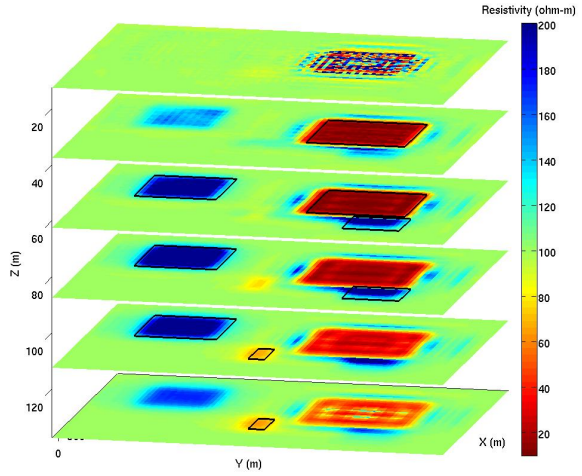

Figure 3: Rigorous inversion result. Notice the depths to the bodies are well resolved, as is the conductivity. This moving footprint rigorous inversion took the same time as the standard LQL inversion.

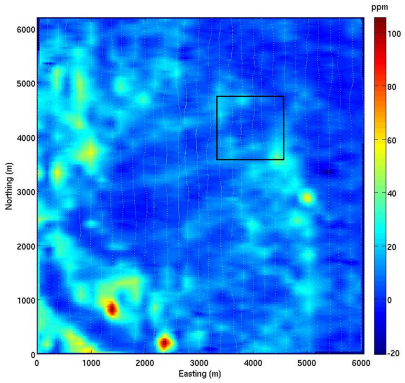

Figure 4: Field data from the 865 Hz inphase coplanar channel. The white dots are sounding locations. Every 10^th location has been taken for a total of about 4,400 soundings per channel. The black box indicates an isolated area with known geology.

30,000 cells. The known target is a resistive target between 0.2 and 0.5 mS/m embedded in a conductive background of around 10 mS/m. The target outcrops and extends to a depth of 80-100 m (A. Foley, personal communication, 2006). Figure 5 shows this structure to be in the correct position.

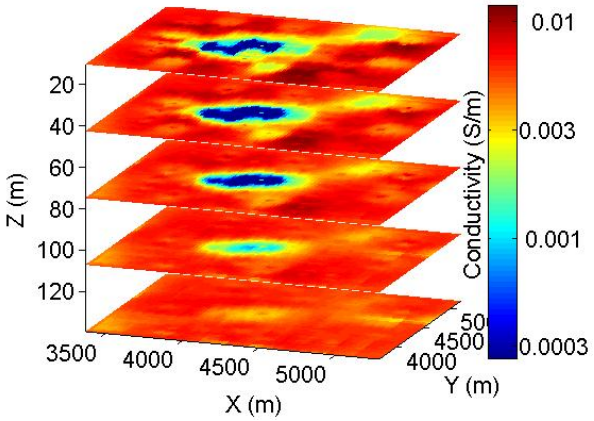

Figure 5: Results of standard LQL inversion over a known structure. This target is known to outcrop and extend to a depth of 80-100m.

The inversion domain is now extended to include the entire survey area (approximately 36 km^2). The inversion included about 20,000 soundings and over 500,000 inversion cells, each a cube 25 m on a side. The results of this inversion are presented in Figure 6, and one can still see the known structure we presented earlier, centered about x=4500 and y=4500 in this inversion. The inversion took approximately 10 hours on a 2.2 GHz AMD 64-bit processor with 4 GB of RAM.

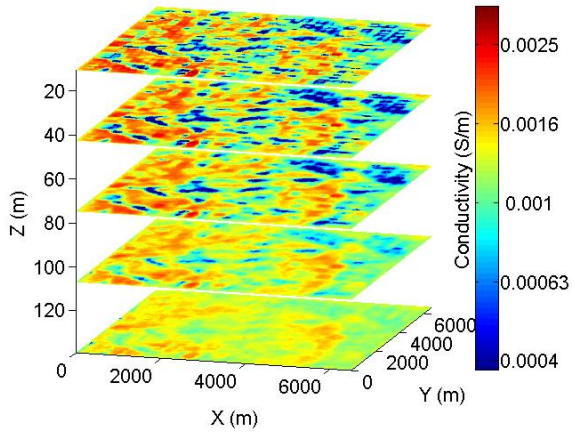

Figure 6: The results of inverting the entire AeroDat survey area. The known structure is still clearly resolved near x=4500, y=4500.

Figure 7 shows a detailed comparison of the inversion results. The results of the two inversions are very similar. The differences arrive from the fact that the second inversion incorporated vastly more data, all of which was included in the global error. Since the inversions were stopped when the global error level in the inversion was reached, the fit of the data points over the known target differed between the inversions.

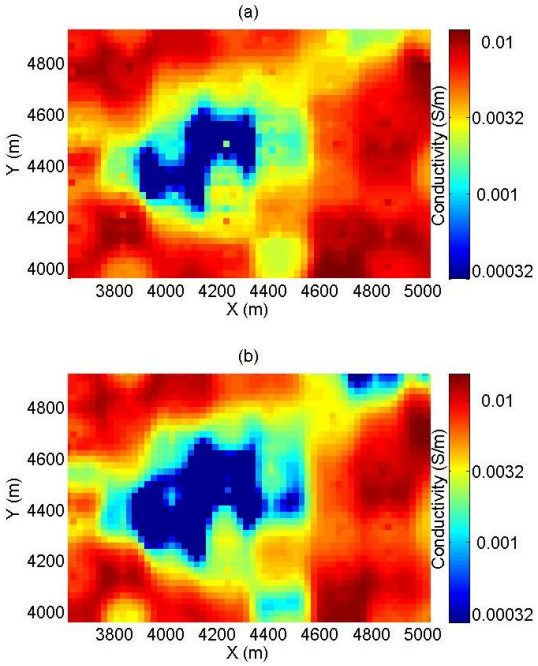

Figure 7: Panel (a) shows the results of standard inversion at a 30 m depth slice. Panel (b) shows a small part of the windowed inversion that extended over the entire domain.

CONCLUSIONS

Windowing the HEM inversion to include only areas near each individual transmitter-receiver pair significantly speeds up inversion, while retaining the accuracy of the original LQL inversion method. With the synthetic model, we have shown this method may be applied to the rigorous inversion method. We have applied this windowing technique to both synthetic and field data: both show accurately recovered models. The field data covered an area in excess of 36 km^2 and contained over 500,000 cells. Over 20,000 stations were included, and the 3D inversion of this data took less than 10 hours on a single PC. Three-dimensional inversion of entire frequency domain helicopter EM data sets is now possible with the techniques presented.

ACKNOWLEDGMENTS

The authors acknowledge the support of the University of Utah Consortium for Electromagnetic Modeling and Inversion (CEMI), which includes BAE Systems, Baker Atlas Logging Services, BGP China National Petroleum Corporation, BHP BillitonWorld Exploration Inc., British Petroleum, Centre for Integrated Petroleum Research, EMGS, ENI S.p.A., ExxonMobil Upstream Research Company, INCO Exploration, Information Systems Laboratories, MTEM, Newmont Mining Co., Norsk Hydro, OHM, Petrobras, Rio Tinto - Kennecott, Rocksource, Russian Research Center Kurchatov Institute, Schlumberger, Shell International Exploration and Production Inc., Statoil, Sumitomo Metal Mining Co., and Zonge Engineering and Research Organization.

We are thankful to Newmont Mining Co. and Dr. Perry Eaton for providing the real geophysical data and for permission to publish the results.

REFERENCES

Beamish, D., 2003, Airborne EM footprints: Geophysical Prospecting, **51**, 49–60.

Cox, L. H. and M. S. Zhdanov, 2006, Rapid and rigorous 3D inversion of airborne electromagnetic data: SEG Technical Program Expanded Abstracts, **25**, 795–799.

Habashy, T. M., R. W. Groom, and B. R. Spies, 1993, Beyond the Born and Rytov approximations - a nonlinear approach to electromagnetic scattering: JGR, **98**, 1759–1775.

Liu, G. and A. Becker, 1990, Two-dimensional mapping of sea-ice keels with airborne electromagnetics: Geophysics, **55**, 239–248.

Reid, J. E., A. Pfaffling, and J. Vrbancich, 2006, Airborne electromagnetic footprints in 1D earths: Geophysics, **71**, G63–G72. 10.1190/1.2187756.

Zhdanov, M. and G. Hursan, 2000, 3D electromagnetic inversion based on quasi-analytical approximation: Inverse Problems, **16**, 1297–1322.

Zhdanov, M. S., 2002, Geophysical inverse theory and regularization problems, volume **36** *of* Methods in Geochemistry and Geophysics: Elsevier.

Zhdanov, M. S. and S. Fang, 1996, Quasi-linear approximation in 3-D EM modeling: Geophysics, **61**, 646–665.

Zhdanov, M. S. and E. Tartaras, 2002, Three-dimensional inversion of multitransmitter electromagnetic data based on the localized quasi-linear approximation: Geophysics Journal International, **148**, 506–519.